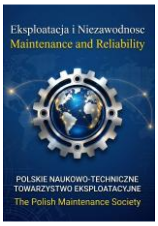

Eksploatacja i Niezawodnosc - Maintenance and Reliability

Volume 29 (2027), Issue 1

https://ein.org.pl

The Polish Maintenance Society

Research on dynamic response and reliability of fuze trigger device action system

Yanan Du[1,*], Guanglin He[1], Xinmin Li[1], Yuzhe Fu[1]

[1] Beijing Institute of Technology, China

* Corresponding Author: fengxiaodan2021@outlook.com

Received: 11 March 2026
Revised: 2 June 2026
Accepted: 11 June 2026
Online: 4 August 2026

Abstract

To improve mechanical actuation systems, this study develops a co-simulation framework to investigate the dynamic response of projec-tile-like trigger device, focusing on firing pin velocity and actuation energy. Based on mechanism analysis, a mathematical model relating structural parameters to piercing velocity is derived for clarifying, the effects of firing pin mass and spring stiffness on dynamic performance. Combined with LSDYNA–ADAMS (Automatic Dynamic Analysis of Mechanical Systems) Monte Carlo co-simulation and experimental validation, motion states and manufacturing tolerances on system reliability are evaluated. Tolerance errors produce a firing-pin velocity range of 24.96–32.93 m/s. After parameter optimization, the velocity range shifts to 28.17–33.68 m/s, enhancing stability. Experimental tests raise the average velocity from 27.53 m/s to 31.27 m/s, vali-dating the proposed method and the quantitative model. This work provides a quantitative basis for tolerance allocation and reliability oriented design of mechanical actuation systems.

Keywords: *mechanical trigger device, virtual shoot-ing, acupuncture speed, machining er-ror, action reliability*

Article citation:
Du Y, He G, Li X, Fu Y, Research on dynamic response and reliability of fuze trigger device action system, Eksploatacja i Niezawodnosc – Maintenance and Reliability 2027: 29(1) http://doi.org/10.17531/ein/224453

Highlights

- This study establishes an LS-DYNA-ADAMS Monte Carlo co-simulation framework.
- Response-based optimization enhances velocity performance and operational reliability.
- The framework features low cost, high computational accuracy, and easy implementation.

1. Introduction

From the perspective of reliability engineering and equipment safety design under extreme conditions, the mechanical trigger system is the core functional unit of the projectile and emergency safety protection device. Its stable and reliable action under transient, strong impact environments is the core basis for determining whether the projectile can complete the preset function and avoid safety accidents caused by function failure, which directly determines the mission reliability and the safety of equipment use. The trigger system's function execution starts with the reliable response of the trigger sequence. As the core energy source and reliability key node of the whole actuation system, the impact energy storage trigger component, whose reliability level directly affects the failure probability and life cycle reliability of the trigger system, is the core control object of equipment reliability design under extreme conditions. Although the technical level of the trigger system continues to improve and the mechatronics integration scheme has been widely used, the traditional pure mechanical trigger structure still has an irreplaceable position in the national defense construction with its core advantages of simple structure, high inherent reliability, low manufacturing cost, and stable operation in various extremely harsh environments such as high temperature, strong impact, and strong electromagnetic interference [1–3]. At the same time, its derivative trigger system has also been continuously promoted in the field of equip-ment. Regarding the dynamic response char-acteristics and reliability of action for mechanical trigger systems, scholars at home and abroad have conducted numerous continuous, in-depth studies [4–7]. The core focuses on the reliability modeling, failure mechanism analysis, and reliability improvement design of the system under extreme conditions, and gradually introduces the datadriven method, PHM technology, and random impact load reliability analysis method to improve the mission reliability and life prediction ability of complex equipment under extreme conditions [8−11]. Wei et al. [12] studied the overall process motion characteristics of the trigger actuation system after projectile launch through theoretical analysis and dynamic simulation. They established a refined dynamic model that in-corporates the system's structural characteristics. The research results show that the model can accurately predict the system action response law, effectively reduce the reliability hidden danger caused by deviation response characteristics, and provide a theoretical basis for the reliability forward design of the mechanical trigger system [13]. Yu et al. [14] established a nonlinear dynamic trans-mission model of the trigger system under strong impact environment by combining numerical simulation and experimental verification for the trigger system under extreme impact conditions, which realized the accurate calculation of the impact overload of the trigger system position, and laid the load input foundation for the dynamic reliability analysis of the system under extreme conditions; The research results show that the relative error between the acceleration peak obtained by the proposed multibody dynamics transfer model and the test results is only 15.7%, which is far lower than the error of 26.4% of the traditional finite element simulation and test results, which greatly improves the calculation accu-racy of reliability analysis and provides a reliable method for the accurate evaluation of system failure probability. Zang et al. [15] carried out the dynamic modeling research of a rigid flexible body coupling system through the combination of numerical calculation and experimental verification, and completed the dynamic response coupling analysis between the trigger system and the carrier in the process of projectile impact. The results show that the accuracy of the calculation method meets the trigger system's reliability design requirements under extreme conditions and effectively captures reliability weak links due to coupling effects. In the field of reliability improvement and high reliability design of trigger actuation systems, relevant research has also been con-tinuously deepened. The core goal is to reduce the system's failure probability and improve its reliability and fault tolerance under extreme conditions. Chang et al. [16] studied the influence of shell material and structural pa-rameters on the action reliability of the trigger system through a numerical simulation method, defined the correlation mechanism between key structural parameters and system reliability, and verified the rationality of this method in the design of system anti impact reliability through experiments, providing a technical path for improving system reliability through structural parameter optimization. Lei and Chen et al. [17,18] conducted impact-resistant optimization design of the core bearing structure of the trigger assembly using finite element analysis. Through the accurate perception of inertia information in the working process, the reliable conversion between the system safety state and the state to be triggered was realized, which greatly improved the intrinsic safety and action reliability of the system, and effectively reduced the occurrence probability of false triggering, nontriggering, and other core failure modes. He et al. [19] proposed a highly integrated trigger actuation system structure through a combination of simulation and experimental verification, enabling reliable on-off control of the trigger circuit via a fast conversion mechanism and reducing the structure height by 44%. The research results showed that the system could complete state conversion within 8 μs and that the state conversion reliability exceeded 99.8%, offering a new scheme for designing a highly reliable trigger system for small equipment. Sharp et al. [20,21] used the failure mode and effect analysis (FMEA) method to systematically sort out the failure mechanism and failure mode of the trigger actuation system, focusing on the impact of key structure, micro size effect and processing technology on the action reliability, established the correlation matrix of system environmental stress and failure mode, and identified the technical path to effectively improve the action reliability of the system by optimizing the structure of the trigger core components; The related research also further shows that improving the technical maturity and structural redundancy of the system and reducing the single fault point are the core direction to improve further the longterm service reliability and life cycle reliability of the trigger system. Xiao et al. [22] showed that when the projectile penetrates the target, a change in load direction due to ballistic de-flection causes an uneven force on the trigger system, leading to fuze failure and reducing system reliability. Through ballistic prediction [23], the projectile's motion can be further analyzed to determine the fuze status, thereby supporting early reliability risk warning. Hui et al. [24] used the numerical simulation method to carry out the system simulation of the trigger mechanism of the fuze, focusing on the analysis of the influence of the structural dimensions of the gasket and bearing on the motion reliability of the trigger mechanism, clarifying the correlation law between the structural parameter deviation and the reliability decline, and optimizing the key structure [25], effectively improving the fuze firing performance and action reliability. Qin et al. [26] studied the influence of the structure of the arming device of the fuze trigger mechanism on the fuze firing reliability. The test verified that fuze firing reliability increased from 89.2% to 98.5%, thereby improving fuze firing efficiency and reliability [27]. Xu et al. [28] studied the correlation between the dynamic response and reliability of the Fuze's internal trigger mechanism through numerical simulation and experimental verification. The research results show that structural optimization of the trigger mechanism parts can im-prove the reliability and safety of the fuze, reduce the fatigue failure probability, and obtain the charge quantity for different structures through structural changes, thereby realizing the collaborative optimization of reliability and performance. Yang et al. [29] studied the impact mechanism of the mechanical structure on the fuze failure under the high overload impact environment through the analysis of the fuze internal buffer parts, and made it clear that the failure of the buffer structure is one of the core factors leading to the decline of the reliability of the trigger system. At the same time, a curved beam structure was proposed to enhance buffer capacity. The simulation and experimental verification showed that the optimized structure can maintain stable energy absorption, reduce the impact damage to the fuze, and improve the reliability of the trigger systems's impact resistance by more than 30%. It is worth noting that system errors generated by part assembly will also reduce the reliability of the trigger system [30], and assembly deviations will lead to stagnation of the trigger component's movement, poor energy transmission, and increased failure risk. Therefore, the reliability control of the assembly process is also an important link in the reliability design of the trigger system. Xu et al. [31] analyzed the damage mechanism of the fuze structure under explosion loading and defined the failure modes and damage thresholds of key parts, thereby laying the foundation for the structural optimization of the fuze and its internal components. Research from other perspectives is also continuously promoting the development of the trigger mechanism. Ren et al. [32,33] studied the minimum ignition energy of the fuze trigger mechanism from the perspective of initiating explosive devices, and developed an initiating explosive device suitable for the structure of the trigger mechanism, reducing the matching error between the initiating explosive device and the trigger mechanism, and improving the ignition reliability. In structural optimization, many scholars have investigated various algorithms [34], with a focus on reliability based design optimization. Chen et al. [35] proposed a Monte Carlo based structural optimization algorithm [36] that quantifies the impact of structural parameter uncertainty on reliability through a random simulation. Experiments show that the algorithm is robust and efficient in real world use, improving the reliability optimization efficiency of the trigger system by more than 40% and demonstrating the Monte Carlo method's efficiency in struc-tural optimization [37]. Ma et al and Chen et al. [38,39] have optimized the contact reliability of precision moving parts under high-speed conditions. While optimizing the extreme environment, it can also scale the environment to achieve reliability optimization for sol-id-structure optimization [40]. In the optimization process, it accounts for the effects on optimization efficiency and reliability improvement [41], thereby achieving collaborative improvements in the reliability and design efficiency of the trigger system. At the same time, the application of machine learning in reliability engineering [42], prediction, and health management (PHM) and life prediction of complex systems is also expanding [43].

To sum up, the existing research has systematically studied the dynamic response characteristics and firing reliability of the fuze trigger mechanism from the aspects of dynamic modeling, impact response analysis, and structural optimization design, and shows that the structural design, key component parameters, and assembly status of the trigger mechanism have a significant impact on the fuze firing performance. However, there is still a lack of systematic research methods and quantitative analysis methods for the dynamic response law of the trigger mechanism and the coupling effect mechanism of key structural parameters on ignition reliability under an extreme impact environment. Therefore, to further elucidate the dynamic response characteristics of the mechanical trigger mechanism under complex impact conditions and their influence on firing performance, this paper takes the mechanical trigger fuze as the re-search object and investigates the trigger mechanism's dynamic response and structural reliability. Firstly, using a multibody dynamics simulation method, the motion response characteristics of the trigger mechanism under typical working conditions are numerically analyzed to obtain its basic dynamic behavior under a single impact condition. Secondly, in combination with the collaborative simulation and experimental verification method, the response research under the virtual firing condition is conducted. By simulating the equivalent firing process of 1000 rounds, the influence of structural parameter changes on the pin's response characteristics is analyzed, and the simulation results are verified against test data to improve the reliability and engi-neering applicability of the model prediction.

2. Analysis of impact-induced dynamic and vibration environment for trigger device actuation

When conducting a kinematic analysis of the triggering environment of the trigger device system, the main focus is on the dynamic analysis of the endpoint trajectory. For ease of analysis, the following assumptions are made:

(1) only consider the forces generated by parts in direct contact with the actuation system parts when analyzing the internal components of the trigger device; this assumption is justified as non-contact structural components have no direct force transmission with the actuation system, and their influence on the internal dynamic response of the actuation system can be neglected, which is a conventional and widely recognized simplification in fuze actuation system dynamic modeling [12,14].

(2) Neglecting the influence of the rotation generated by the projectile-like mechanical structure during flight on the actuation system; this assumption is justified as the test is conducted under a non-spinning launch condition, and the centrifugal force generated by low residual rotation is far less than the axial impact overload during target penetration, thus having a negligible effect on the axial motion of the actuation system components.

(3) Due to the extremely small gap be-tween the firing pin and the firing pin seat, the offset error between the firing pin and the main structure axis is ignored. This assumption is justified because the fit clearance between the firing pin and the guide seat is controlled to within 0.02 mm in actual machining, and the radial offset is much smaller than the firing pin stroke, so it will not affect the axial motion characteristics of the firing pin. Similarly, to establish a complete dynamic model of the actuation system, without simplifying the parts, when the projectile-like mechanical structure collides with the target at a small angle, the dynamic model of the actuation system is shown in Figure 1, and the red position on the firing pin is the center of mass position of the firing pin. When the projectile-like mechanical structure impacts the target at a small angle, the trigger device is subjected to a strong impulsive load, which can be regarded as a transient shock excitation that induces high-frequency vibration responses in the internal components.

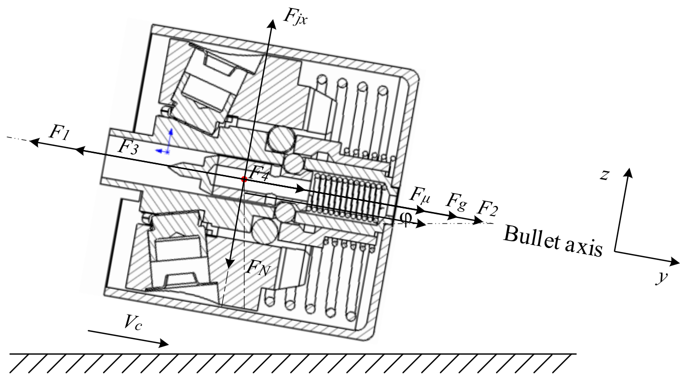

Figure 1. Schemetic Motion analysis of initiation system.

Before hitting the target, the actuation system remains in a dynamic equilibrium state without any radial load, and both the inertial block and firing pin are in a balanced state.

$$\begin{cases} F_1 + F_2 = 0 \\ F_3 + F_4 = 0 \end{cases} \tag{1}$$

In the formula, F_1 is the preload force of the inertial block spring; F_2 is the sup-port force of the device cover on the inertial block; F_3 is the preload force of the firing pin spring, and F_4 is the support force of the steel ball on the firing pin.

When a projectile-like mechanical structure collides with a target at a small angle, it is subjected to a reaction force from the target. The inertial block overcomes the spring's pretension and rushes forward, then releases the steel ball. The firing pin pierces the actuation component under the action of the firing pin spring. In the direction of the projectile-like mechanical structure axis, the firing pin only needs to overcome the frictional force on the side wall to move.

$$m_2\ddot{x} = R_0 - F_\mu \tag{2}$$

where m_2 is the mass of the firing pin, $\ddot{x}$ is the axial acceleration of the firing pin, R_0 is the elastic force of the firing pin spring, and F_μ is the sliding friction between the firing pin and the guide seat.

The force acting on the actuation system's firing pin piercing the actuation component is the basis for determining the movement of the firing pin. When studying the firing pin piercing the actuation component, the mechanical environment of the inertial block and the firing pin is different. After colliding with the target, when the reactive force of the target is released, the inertial block rushes forward. At this time, the inertial block is subjected to inertial forces, frictional forces between parts, spring resistance of the inertial block, and radial forces generated by colliding with the target. After the inertial block completes the forward thrust, the movement of the sliding sleeve will introduce a delay of about 210 μs. After the sliding sleeve motion is completed, the firing pin is driven by the spring force of the firing pin spring to puncture the actuation component. The impact environment when hitting the target affects the activation of the inertial block. When the firing pin pierces the actuation component, the pretension force of the inertial block spring and the firing pin's factors will affect the actuation system's response speed and time. The force model is shown in Figure 2.

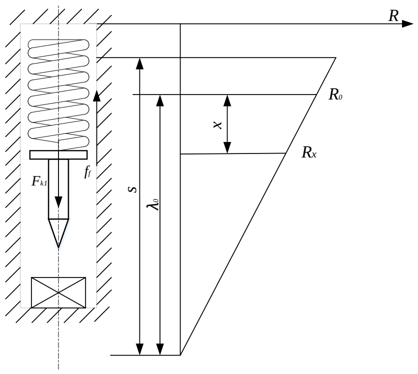

Figure 2. Force diagram of the initiation system firing pin.

As shown in Figure 2, after the firing pin is released, it moves toward the actuation component by a stroke of x. The spring resistance acting on the firing pin is:

$$R_x = \frac{R_0}{\lambda_0}(\lambda_0 - x) \tag{3}$$

where R_0/λ_0 is the stiffness of the firing pin spring, and x is the pre-compression of the firing pin spring in the assembled state.

The frictional force generated by radial overload is:

$$F\mu = f_c + \mu m_2 a_r \tag{4}$$

where f_c is the static Coulomb friction between the firing pin and the guide seat, μ is the sliding friction coefficient, and a_r is the radial overload of the system.

The kinematic expression of the firing pin is:

$$m\frac{d^2x}{dt^2} = R_x - F_\mu = \frac{R_0}{\lambda_0}(\lambda_0 - x) - F_\mu \tag{5}$$

Based on the above kinematic equation, combined with Newton's second law and the kinetic energy theorem, an explicit quantitative mathematical model for the puncture speed V and key structural parameters when the striker reaches the end face of the actuator is derived.

The movement process of the hammer pin is solved by integration. The total stroke of the hammer pin from release to contact with the actuating element is s. in this paper, s = 5.98 mm. During the movement process, the spring force does positive work, and the friction force does negative work, ignoring the secondary energy loss. According to the kinetic energy theorem:

$$\int_0^s k_1\,(x_0 + x)dx - \int_0^s f\,dxR_x = \frac{1}{2}m_2v^2 \tag{6}$$

where: k_1 is the spring stiffness of the striker, x_0 is the preload shrinkage of the striker spring, f is the average sliding friction caused by radial overload, and v is the puncture speed when the striker contacts the actuating element.

The above formula is simplified, and the explicit expression of puncture speed is obtained:

$$v = \sqrt{\frac{k_1(2x_0s + s^2) - 2fs}{m_2}} \tag{7}$$

The mathematical model directly quantifies the influence of the needle spring stiffness k_1 and the needle mass m_2 on the puncture speed v: the puncture speed is positively correlated with the square root of the needle spring stiffness, and negatively correlated with the square root of the needle mass, which is completely consistent with the parameter influence law obtained in section 4.4 of this paper, and realizes the quantitative characterization of the influence of key parameters on the dynamic response of the system.

According to the actuation component model of the actuation system, the minimum activation energy is 7.07 mJ, and the depth of the firing pin punched actuation component is at least 1.27 mm. The complete derivation of the critical velocity threshold for reliable activation is carried out based on the law of energy conservation as follows:

$$E_{k,min} = E_{min} \tag{8}$$

where $E_{k,min}$ is the minimum kinetic energy of the firing pin, and E_{min}=7.07 mJ is the minimum activation energy of the actuation component given by the product model.

The kinetic energy of the firing pin is calculated by the classical kinetic energy formula:

$$E_k = \frac{1}{2} m_2 v^2 \tag{9}$$

where m_2 is the nominal mass of the firing pin, which is 0.12 g, consistent with the nominal value in Section 4.2 of this paper. Substitute the critical state condition $E_k = E_{min}$ into Equation (8), and rearrange to obtain the analytical expression of the critical velocity v_{min}:

$$v\sqrt{\frac{2E_{min}}{m_2}}_{min} \tag{10}$$

Substituting the known parameters E_{min} = 7.07 mJ and m_2 = 0.12g into Equation (10), the critical speed is 10.86 m/s.

This critical velocity is the minimum value to ensure that the firing pin can provide sufficient activation energy and reach the required minimum piercing depth of 1.27 mm. When the velocity is not less than 10.86 m/s, it can be fully activated. This speed threshold is the core index for ensuring the reliability of the actuation system's actions.

3. Kinematic simulation

In this section, a finite element simulation of a projectile-like mechanical structure penetrating a sandbag target is performed to obtain the actuation system's overload curve, which is used as the overload input for the actuation system's dynamic simulation. Then, the motion process of the actuation system is obtained, providing accurate simulation data support for the subsequent reliability analysis of the actuation system.

3.1. Finite element simulation

3.1.1. Finite element model

Establish a finite element model of a projectile-like mechanical structure penetrating sandbag targets, treating sandbags as mean targets. The obtained overload curve represents the transient shock excitation acting on the trigger device during target impact and serves as the primary vibration input for the subsequent dynamic response analysis of the actuation system. Its simulation accuracy directly affects the reliability analysis of the actuation system.

In finite element simulations, the number and quality of grids affect calculation accuracy and time. The higher the similarity between the grid shape and the standard shape, the higher the calculation accuracy. To obtain accurate simulation results, both the 3D and finite element models were 1:1 for the projectile-like mechanical structure, trigger device structure, and energy storage structure. The target medium used a hexahedral mesh, and the precise structures of the projectile-like mechanical structure and fuze used tetrahedral and hexahedral meshes with a mesh size of 2 mm and a total of 641659 elements. The internal components of the rigger device are in a discrete state, and the natural state of the target is described by setting a non-reflective surface around the target medium. The finite element model of the projectile-like mechanical structure hitting the sandbag target is shown in Figure 3. The length of the sandbag target plate is 2.5 m, the thickness is 0.5 m, and the numerical simulation calculation unit is cm-g-μs.

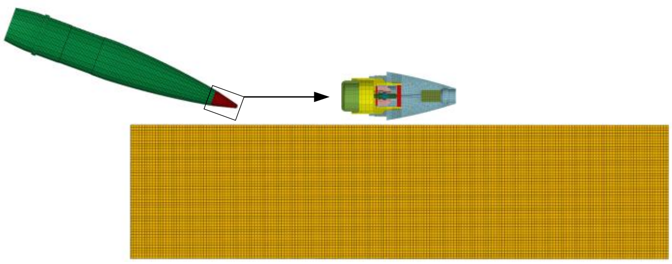

Figure 3. Finite element model.

3.1.2. Material model

The MAT_JOHNSON_COOK model can accurately characterize the mechanical behavior of metal materials over a wide range of strain rates, from low strain rate quasi-static conditions to high strain rate impact conditions. Typical applications include explosive metal forming, ballistic penetration, and impact problems [14,16]. In the numerical simulation, isotropic elastic-plastic materials are used to model the mechanical properties of the mechanical structure, trigger device, and other components of a similar projectile.

Typical applications include explosive metal forming, ballistic penetration, and impact problems. In the numerical simulation, isotropic elastic-plastic materials are used to model the mechanical properties of the mechanical structure, trigger device, and other components of a similar projectile. During the impact process, the projectile and trigger device may be slightly damaged, accompanied by large strain and high strain rate. Therefore, *The MAT_JOHNSON_COOK model in LS-DYNA is selected to describe the mechanical properties of metal materials, which can accurately characterize the mechanical behavior of materials under extreme impact conditions and provide reliable material parameter support for the reliability simulation of the actuation system. The model considers the effects of strain hardening, strain rate hardening, and temperature softening simultaneously. When combined with the rate equation in the yield surface, the performance description includes the initial yield stress, hardening constant, dimensionless hardening coefficient, dimensionless temperature, and other parameters. The stress formula is as follows:

$$\sigma_y = \left(A + B\varepsilon_p^n\right)\left(1 + C\, ln\, \dot{\varepsilon}^*\right)[1 - (T^*)^m] \tag{11}$$

In the formula, A, B, n, C, and m represent the initial yield strength, strain strengthening index, strain rate sensitivity coefficient, hardening index, and temperature softening index, respectively. These material parameters are usually determined through experiments. ε_p is he effective plastic strain, $T^* = (T - T_r)/(T_m - T_r)$ is the effective plastic strain rate, is the same series temperature, T is the current temperature, T_m and T_r are the melting temperature and room temperature, respectively. Due to the nonlinear dependence of flow stress on plastic strain, the accurate value of model stress requires iterative increments of plastic strain. However, by using a linearized Taylor series expansion of the current time, the solution can be solved with sufficient accuracy to avoid iterations.

The failure strain is as follows:

$$\varepsilon_f = \left[D_1 + D_2 e^{D_3\sigma^*}\right][1 + D_4\, ln\, \varepsilon^*][1 + D_5 T^*] \tag{12}$$

In the formula, D_1, D_2, D_3, D_4, and D_5 are the failure parameters, σ^* is the ratio of pressure to effective stress, $\sigma^* = p/\sigma_{eff}$, and when $D = \sum \Delta\bar{\varepsilon}^p/\varepsilon^f = 1$ occurs, the material fails. To describe the state at high strain rates, the Gruneisen equation of state is used, which defines the pressure of the material as:

$$p = \begin{cases} \dfrac{\rho_0 C^2 \mu\left[1 + \left(1 - \frac{\gamma_0}{2}\right)\mu - \frac{a}{2}\mu^2\right]}{\left[1 - (S_1 - 1)\mu - S_2\frac{\mu^2}{\mu+1} - S_3\frac{\mu^3}{(\mu+1)^2}\right]^2} + (\gamma_0 + a\mu)E & (\mu \geq 0) \\ \rho_0 K^2 \mu + (\gamma_0 + a\mu)E & (\mu \leq 0) \end{cases} \tag{13}$$

In the formula, C is the intercept of $(v_s - v_p)$'s curve; S_1 is the slope coefficient of the v_s-v_p curve, v_s is the impact velocity, v_p is the particle velocity; γ_0 is the dimensional parameter of the Gruneisen equation; a is the first-order volume correction for γ_0, $\mu = \rho/\rho_0 - 1$, E is the internal energy.

The material model parameters of components such as projectiles and trigger devices are shown in Table 1.

Table 1. Metal material parameter settings.

Material	*A*(MPa)	*B*(MPa)	*n*	*C*	*m*	T_m (K)	T_r (K)	c_0 (cm/μs)	*S*
Alloy steel	792	180	0.12	0.016	1.0	1520	294	0.458	1.33
Aluminum alloy	102	50	0.19	0.001	0.859	893	293	0.3	-

The sandbag is described using the *MAT_SOIL_AND_FOAM model, and its material parameters are listed in Table 2. Since there is no failure in this model, the definition of failure is introduced using *MAT_ADD_EROSION. Ensure that the damage characteristics of the sandbag target are consistent with the actual situation during the simulation, and improve the reliability of the overload curve simulation.

Table 2. Sandbag material parameter settings.

Parameter	RO	G(MPa)	K(Mpa)	A_2
Numerical value	1.30	1.724	5.516	0.87

3.1.3. Finite element results

The collision of a projectile with a sandbag target belongs to the impact problem, and the Lagrange algorithm is the most widely used method for solving explosion and impact problems [14,15]. The material of the Lagrangian algorithm is attached to the grid, tracking the flow of each mass point, that is, the grid and material deform deform together. Therefore, this algorithm is easy to determine the time history, as well as the material structure interface and the internal stress train state. Therefore, the Lagrangian algorithm can simulate the dynamic behavior of solid materials well. In conjunction with the Lagrangian algorithm, the contact between the projectile and the semi infinite thickness target adopts surface erosion contact, and the contact between the trigger device and the semi infinite thickness target also adopts surface erosion contact, with a contact stiffness of Finite Element Results.

The process of the projectile-like mechanical structure penetrating the sandbag at a 30° incidence angle is shown in Figure 4.

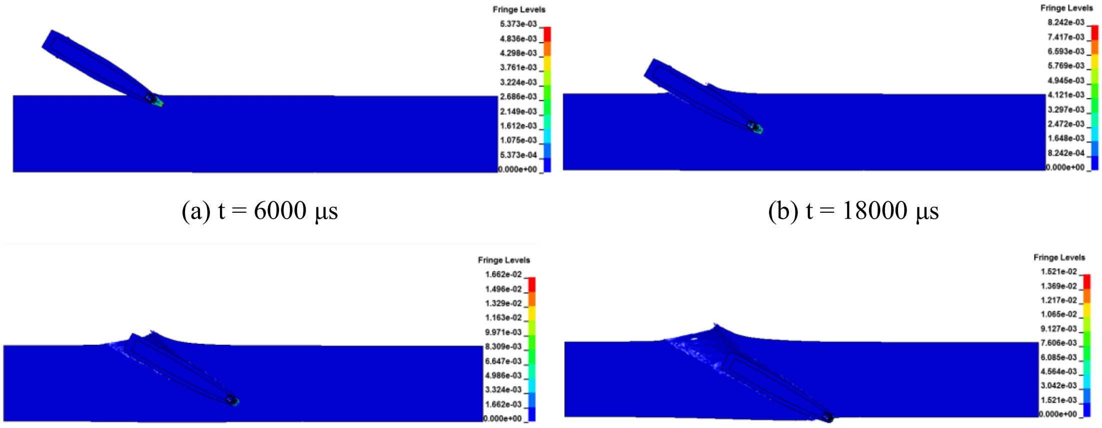

(a) t = 6000 μs (b) t = 18000 μs

(c) t = 27000 μs (d) t = 36000 μs

Figure 4. Finite element simulation results of a projectile-like mechanical structure penetrating a sandbag target.

From the numerical simulation results in Figure 4, it can be seen that the simulation captures the projectile penetrating the sandbag at a small angle. When t = 6000 μs, the projectile-like mechanical structure has penetrated, resulting in microcracks and relaxation zones in the shallow material on the target surface. At this time, the contact reaction and normal deceleration rise rapidly; When t = 18000 μs, the projectile-like mechanical structure penetrates continuously, with the lateral material outflow, the surface forms a continuous shallow groove, the contact line moves backward along the shape of the projectile-like mechanical structure, the contact area increases, the friction resistance and tangential energy dissipation ratio increase, and the normal bearing tends to be flat; When t = 27000 μs, the projectile-like mechanical structure completely penetrates, and the deceleration of the projectile-like mechanical structure is obvious with the decrease of the angle between the projectile-like mechanical structure axis and the target surface; When t = 36000 μs, the front-end structure passes through the target plate, the contact reaction force and normal compaction continue to decay, the stress wave in the target body attenuates to the far field, and the local damage enters the stress drop stage. The trigger device overload curve is shown in Figure 5. The curve provides accurate load input for the dynamic response and reliability analysis of the subsequent actuation system.

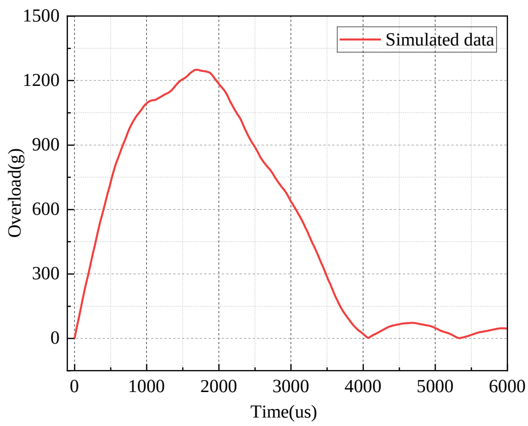

Figure 5. Trigger device overload curve.

3.2. Simulation of the actuation system

3.2.1. Dynamic simulation

Dynamic modeling was conducted on the actuation system, using the trigger device overload when the projectile-like mechanical structure hits the sandbag target as input. ADAMS software was used to simulate the actuation system's kinematics, and the resulting dynamic model is shown in Figure 6.

All kinematic pairs and constraints are strictly defined in full accordance with the actual assembly relationship of the trigger mechanism: (1) The outer shell of the mechanism is fixed to the global coordinate system via a Fixed Joint, to simulate the actual installation constraint of the device; (2) A Translational Joint is applied between the inertial block and the shell, which only allows the inertial block to move along the axial direction of the projectile; (3) A Cylindrical Joint is adopted between the firing pin and the shell guide hole, which limits the radial offset of the firing pin and only retains its axial translational degree of freedom; (4) The preload and stiffness of the inertial block spring, sliding sleeve spring and firing pin spring are applied through the Spring Force element built in ADAMS, with parameter ranges completely consistent with those in Table 3 of this paper; (5) The steel balls retain 6 degrees of freedom in the free state before release, and are constrained by contact force after contacting with the limiting structures.

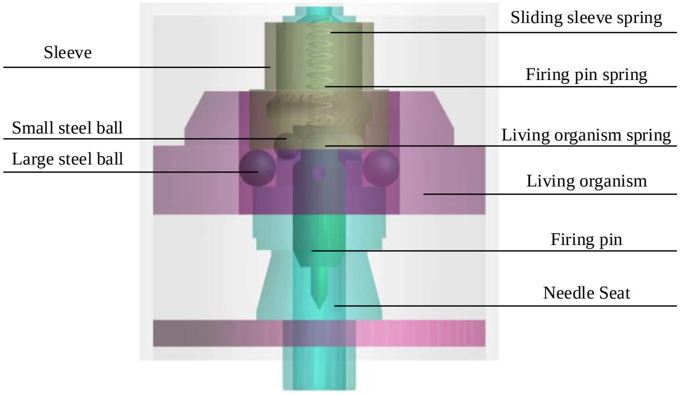

Figure 6. Dynamic model.

The contact between the metal components of the mechanism is defined by the builtin Impact rigid contact algorithm in ADAMS, which is suitable for highprecision simulation of impact contact under overloading conditions. The key contact pairs in the model include: inertial block and steel balls, steel balls and firing pin limiting groove, firing pin and shell guide surface, sliding sleeve and shell. The contact parameters are set according to the alloy steel properties of the actual parts (as shown in Table 1): the contact stiffness coefficient is 1.2×10^5 N/mm, the damping coefficient is 50 N·s/mm, the collision index is 2.2, and the maximum allowable penetration depth is 0.01 mm.

The measured penetration overload curve (Fig. 5) obtained from LS-DYNA finite ele-ment simulation is used as the excitation input of the model, and the specific application method is as follows: (1) The timedomain overload data is imported into ADAMS as discrete data points, and fitted to generate a SPLINE spline curve; (2) The axial acceleration excitation is applied to the mass center of the fixed shell along the projectile axis through the AKISPL interpolation function, to reproduce the actual impact overload environment during target collision accurately; (3) The total simulation time is set to 4 ms, and the solution step size is set to 1 μs, which fully covers the whole action process of the mechanism and ensures the calculation accuracy of the highspeed impact dynamic response.

The ADAMS kinematic simulation process is shown in Figure 7. According to the previous text, it can be concluded that when the velocity of the firing pin piercing the actuation component exceeds 10.86 m/s, the actuation component's activation performance requirements are met. The speed threshold is the core index for assessing the reliability of the actuation system's actions.

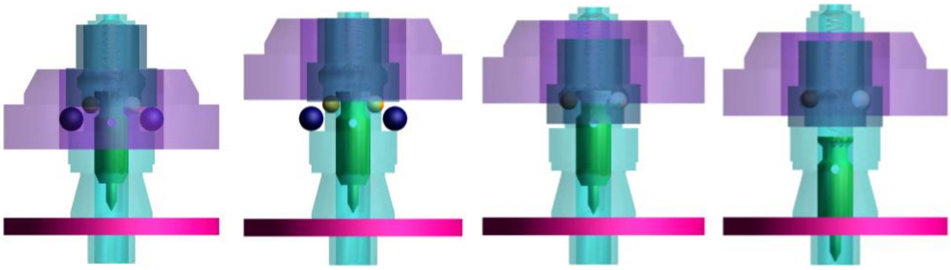

(a) Initial state (b) t = 1700 μs (c) t = 3600 μs (d) t = 3900 μs

Figure 7. Dynamic simulation of the firing pin piercing actuation component.

The forward thrust of the inertial block under inertial force is the beginning stage of the activation process, while the firing pin piercing the actuation component is the end stage of the activation motion. The capture of the inertial block's activation and the speed of the firing pin piercing the actuation component at the beginning of the activation motion serve as the basis for reliable activation of the entire actuation system. According to Figure 7, when t = 1700 μs, the inertial block moves in place and releases the large steel ball; When t = 3600 μs, the sliding sleeve moves downwards to align with the small steel ball in the slot, releases the small steel ball, and releases the firing pin; When t = 3900 μs, the firing pin moves downward to a certain position until it hits the actuation component.

3.2.2. Simulation results

The velocity and displacement curves of the firing pin, obtained from ADAMS kinematic simulation after the trigger device contacts the target, are shown in Figure 8.

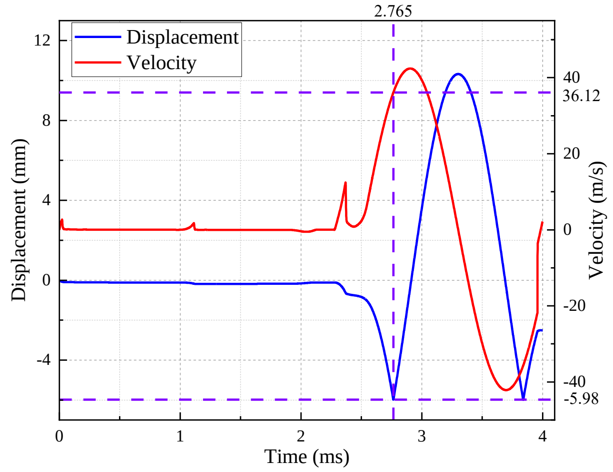

Figure 8. Needle velocity displacement curve.

At the initial position, the distance between the firing pin and the actuation component is 5.98 mm. As shown in Figure 8, the simulation results indicate that at 2.765 ms, the firing pin's displacement reaches 5.98 mm. Therefore, at this time, the firing pin pierces the actuation component at a speed of 36.12 m/s, which is higher than the minimum speed of 10.86 m/s for piercing the actuation component and meets the activation performance requirements. From a kinematic perspective, only by overcoming the displacement between the firing pin and the actuation component can the firing pin pierce the actuation component. The shorter the time to reach maximum displacement, the higher the probability that the trigger device is reliably activated. This rule provides an important basis for the reliability optimization of subsequent actuation systems.

4. Simulation of response law of actuation system

In this section, Monte Carlo simulation, DOE (Design of Experiments) simulation, variable optimization, and output variable analysis and verification after variable optimi-zation are carried out for the actuation system, focusing on the impact of structural parame-ters on the action reliability of the actuation system, and a reliability optimization scheme is proposed.

4.1. Co-simulation model

Based on the design dimensions of the trigger device, the speed of the firing pin piercing the actuation component is extracted to determine whether the trigger device can be activated, and the influence of variables on the actuation system is then determined. The cross-platform collaborative model of the trigger device actuation system is shown in Figure 9, and the operation process is shown in Figure 10.

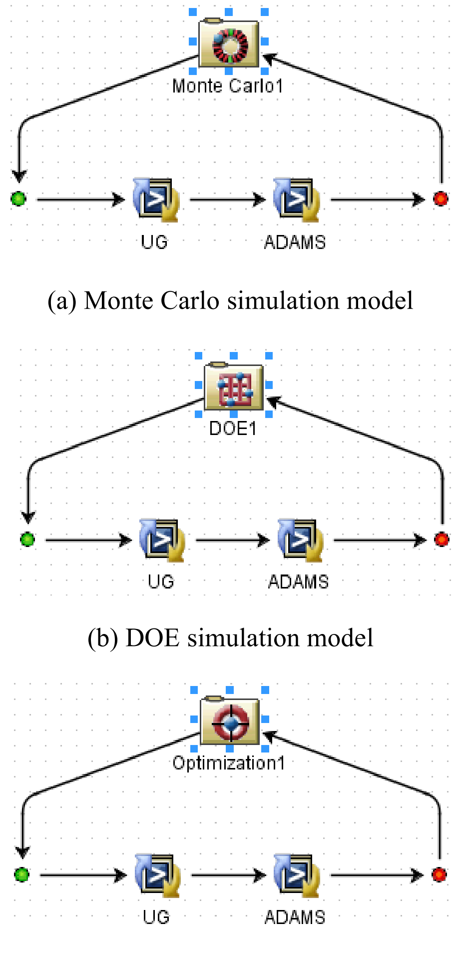

Figure 9. Cross platform collaborative simulation model.

In Figure 9, (a) is the Monte Carlo simulation model, (b) is the DOE simulation model, and (c) is the variable optimization simulation model. Conduct 1000 sets of virtual impact tests experiments using Monte Carlo simulation models, with varying ranges of output variables; Analyze 1000 sets of virtual impact test data through DOE simulation model, determine the impact of input variable changes on output variables, and thus obtain the response law of output variables; By optimizing the simulation model through variables, the output variables that meet the requirements are obtained by optimizing the input variables, and then the optimized input variables are verified.

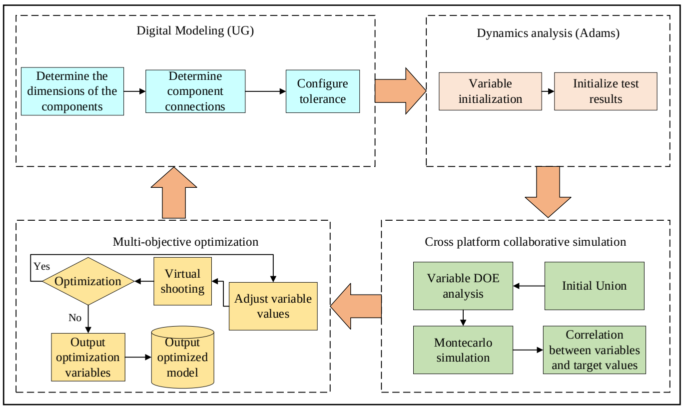

Figure 10. Simulation framework process.

4.2. Input variable

In the movement of the actuation system, the movement of the inertial block, sliding sleeve, and firing pin are all influenced by their corresponding springs. The inertial block spring, sliding sleeve spring, and firing pin spring play an important role in the overall movement of the actuation system. The length of the firing pin spring under no pressure is 17.58 mm. When the compression amount is 7.7mm, due to processing errors, the spring force is 13.24 N~15.86 N. The spring stiffness is calculated by $k = F/\delta$, where F is the spring force and δ is the compression amount. Therefore, the maximum stiffness of the firing pin spring is 2.06 N/mm, and the minimum stiffness is 1.72 N/mm. When the compression amount is 5.89 mm, due to processing errors, the spring force is 4.18 N~4.76 N. The stiffness is also calculated by $k = F/\delta$. Therefore, the maximum stiffness of the sliding sleeve spring is 0.81 N/mm, and the minimum stiffness is 0.71 N/mm. The length of the inertial block spring under no pressure is 59.69 mm. When the compression amount is 4.19 mm, the spring force is 0.5 N~0.6 N due to processing errors. The stiffness is calculated by $k = F/\delta$ to ensure the accuracy. Therefore, the maximum stiffness of the inertial block spring is 0.144 N/mm, and the minimum stiffness is 0.119N/mm.

Under the nominal size, the sliding sleeve has a total height of 9.44 mm and a diameter of 10.41mm under the nominal size, with a machining error of -0.03 mm~+0.03 mm. By maximizing and minimizing the sliding sleeve's size, the maximum mass is 1.722 g, and the minimum is 1.588 g. The total length of the firing pin is 13.97 mm, the diameter is 3.65 mm, and the machining error is -0.05 mm~+0.05 mm. By maximizing and minimizing the firing pin's size tolerance, the maximum mass is 0.126 g, and the minimum is 0.114 g. These variables are the core factors that affect the reliability of the actuation system action and are also the key targets of subsequent optimization. Convert the tolerance of the trigger device initiation system components into mass and spring stiffness as input variables, as shown in Table 3.

Table 3. Variable factor input range.

Variable factor	Parameter	
	Lower limit	Upper limit
k_1 (Firing pin spring stiffness)	1.72 N/mm	2.06 N/mm
k_2 (Sliding sleeve spring)	0.71 N/mm	0.81 N/mm
k_3 (Inertial block spring)	0.119 N/mm	0.144 N/mm
m_1 (Sliding sleeve quality)	1.588 g	1.722 g
m_2 (Firing pin quality)	0.114 g	0.126 g

4.3. Virtual test results

To verify the influence of variables on the activation performance of the actuation system, Monte Carlo simulation was conducted on the trigger device actuation system. Descriptive sampling and normal distribution were used to determine the values of each variable, with a simulation quantity of 1000 groups. The speed of the firing pin piercing, the distribution of actuation components in the trigger device, and the actuation system after simulation are shown in Figure 11.

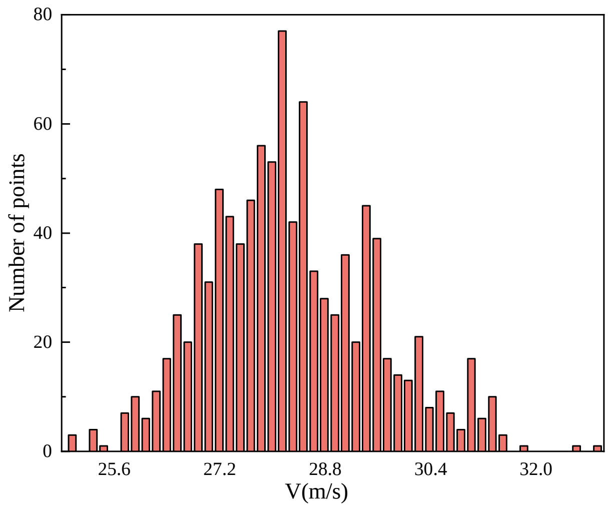

Figure 11. Firing pin piercing detonator speed.

According to the previous text, it can be seen that the actuation system can achieve reliable activation when the firing pin piercing speed of the actuation component under nominal size must be greater than 10.86 m/s. According to Figure 11, the velocity range of the firing pin piercing the actuation component is 24.96~32.93 m/s, which is much higher than the minimum activation velocity. By optimizing the parameters at the tolerance level, the range of firing pin piercing speed can be reduced, thereby narrowing the distribution of activation points and improving the prediction of damage effects. Improve the action reliability and consistency of the actuating system.

4.4. Analysis of factors affecting firing pin speed

From the perspective of impact, manufactur-ing tolerance introduces uncertainty into the dynamic response of the actuating system, leading to a random distribution of striker speed under the same impact excitation and directly affecting the reliability and consistency of the actuating system. Based on the second order regression analysis of 1000 groups of virtual impact tests, the main effect and contribution rate diagrams are shown in Figure 12.

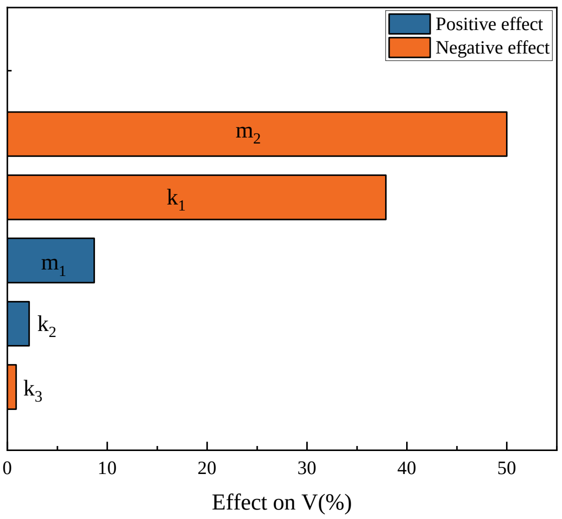

(a) Contribution rate of variables

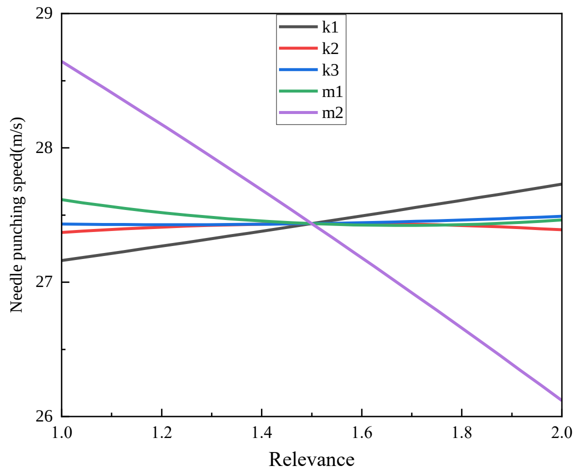

(b) Main effect diagram

Figure 12. Variable analysis results.

In Figure 12, (a) is the contribution rate chart of variables to the speed of firing pin piercing actuation components; (b) is the main effect diagram of variables on the speed of firing pin piercing actuation components. According to Figure 12, the mass m_2 of the firing pin has the largest contribution to the speed of the firing pin piercing the actuation component, at 49.98%. The second most influential variable factors are the spring stiffness k_1 of the firing pin and the mass m1 of the sliding sleeve, with contribution rates of 37.89% and 8.69%, respectively. Among them, the mass m_2 of the firing pin is negatively correlated with the speed of the firing pin piercing the actuation component, the stiffness k_1 of the firing pin spring is positively correlated with the speed of the firing pin piercing the actuation component, the mass m1 of the sliding sleeve and the stiffness k_2 of the inertial block spring are positively correlated with the speed of the firing pin piercing the actuation component, and the stiffness k_3 of the sliding sleeve spring is negatively correlated with the speed of the firing pin piercing the actuation component. This parameter influences the law, which is completely consistent with the quantitative mathematical model derived in Chapter 2 of this paper, which verifies the accuracy of the mathematical model, and realizes the promotion from the simulation test law to the theoretical quantitative model, which can provide a theoretical basis for the parameter design of similar mechanical actuation systems. This puts forward new requirements and directions for subsequent optimization design. It points out the direction for reliability optimization of the subsequent actuation system.

4.5. Dynamic performance optimization

4.5.1. Variable optimization

The optimization objective is to maximize the mean firing pin piercing velocity and narrow the velocity distribution range to improve the action reliability and consistency of the actuation system. Based on the contribution of variable factors to response time in the previous text, the key variables m_2 and k_1 were optimized. The optimization process is shown in Figure 13.

According to Figure 13, under this operating condition, the number of iterations for variable optimization is 178, and the global search for the optimal solution occurs at step 135, with m_2 = 0.122 g and k1 = 1.88 N/mm.

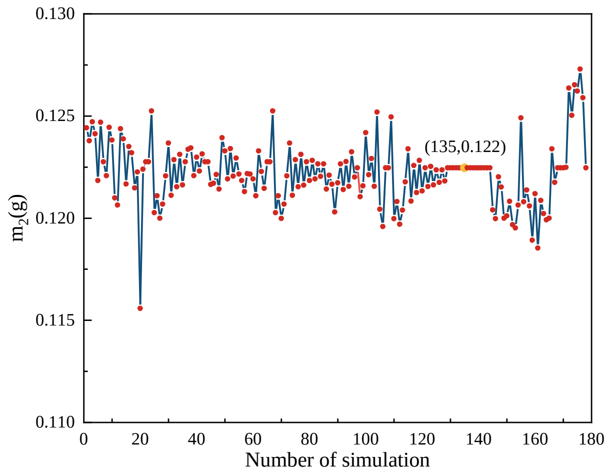

(a) The optimization process of m_2

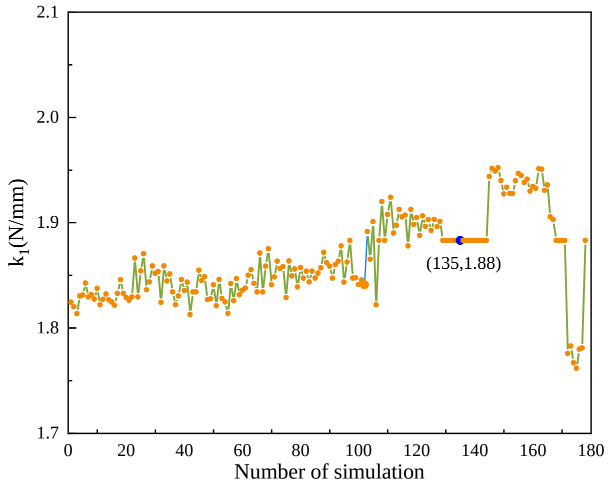

(b) The optimization process of k_1

Figure 13. Variable iteration optimization process.

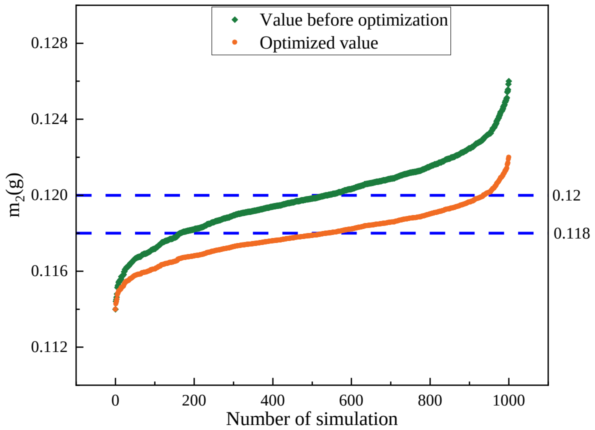

(a) Range of values before and after m_2 optimization

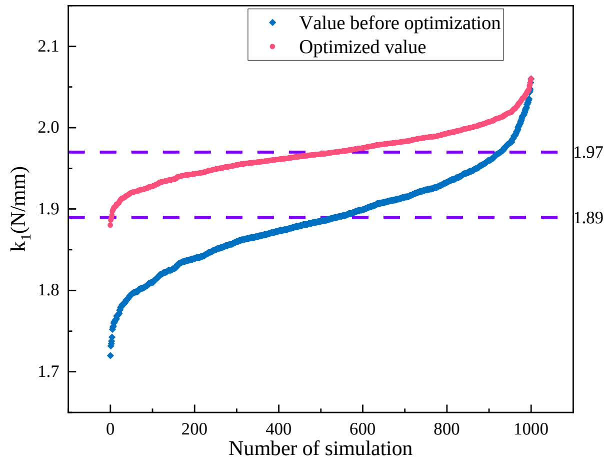

(b) Range of values before and after k_1 optimization

Figure 14. Variable distribution before and after optimization.

4.5.2. Optimized results

The distribution of variable factors before and after the optimization process is shown in Figure 14.

For the firing pin mass m_2, the mass is slightly reduced after optimization with a relative change of only 1.67%, which can be achieved by adjusting the diameter or length of the firing pin head in engineering practice. For the spring stiffness k_1, there is a slight difference between the theoretical optimized value and the engineering realizable value. Finally, 1.97 N/mm is adopted as the actual nominal stiffness, with a relative change of 4.32%, which is still within the conventional tolerance range of spring manufacturing. The refined parameter set modifies the dynamic response characteristics of the system while remaining fully within the specified geometric machining tolerance constraints. This demonstrates both the physical interpretability and practical applicability of the proposed optimization method.

Table 4. Comparison of key structural parameters before and after optimization.

Variable	Baseline nominal	Optimized nominal	Nominal	Absolute change	Relative change (%)
m_2	0.12 g	0.118 g	0.116 g	0.002	1.67
k_1	1.89 N/mm	1.88 N/mm	1.97 N/mm	0.06 N/mm	4.32

4.5.3. Optimization verification

Through multivariate optimization, the optimized variable factors were used as inputs to further verify the actuation component's firing pin-piercing energy and the actuation system's instantaneous activation rate. Comparative simulations were conducted using the optimized nominal parameters (m_2 = 0.118 g, k_1 = 1.97 N/mm) to quantitatively validate the optimization effect. The optimized results are shown in Figure 15.

From Figure 15, it can be seen that after optimizing the variable factors, the speed of the driving needle piercing the driving component of the driving system significantly increased from 24.96~32.93 m/s to 28.17~3 3.68 m/s, and the range difference decreased from 7.97 m/s to 5.51 m/s, a decrease of 31%. The comparative results confirm that adjustments to m_2 and k_1 effectively improve performance, and the speed distribution is more concentrated and more stable. The initial reliability and consistency of the driving system were further improved, thereby verifying the effectiveness of the optimization scheme and providing technical support for its reliability design.

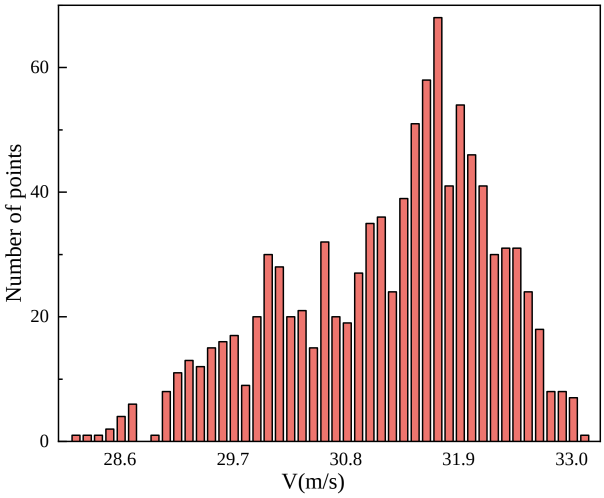

Figure 15. Optimized firing pin piercing actuation component speed.

5. Experimental verification

In order to verify the accuracy of the simulation analysis and the effectiveness of the optimization methods, a trigger mechanism testing system was designed, including a trigger device overload testing system, a live organism startup detection system, and a needle piercing speed testing system. The experimental conditions are: the mechanical structure of the projectile impacts the sandbag target plate at a 30 ° angle and a speed of 330 m/s. The experiment mainly verifies the accuracy of the simulation results of the impact overload of the triggering device, the starting process of the living organism, the reliability of the triggering mechanism, and the influence of key variables k_1 and m_2 on the firing needle speed before and after optimization.

5.1. Storage testing system

After the storage testing system is powered on, it will collect realtime acceleration and firing needle velocity signals from the projectile's mechanical structure at a high sampling frequency. The obtained sensor output signal is processed by the signal conditioning circuit and A/D conversion, and then digitally processed by the main controller and stored in the system memory. When the triggering mechanism meets the actuation conditions, the system enters a cyclic sampling state and records key data. After data collection is completed, the system automatically enters a low power state and waits for data retrieval before reading. The system architecture diagram is shown in Figure 16.

The hardware of the testing system is shown in Figure 17.

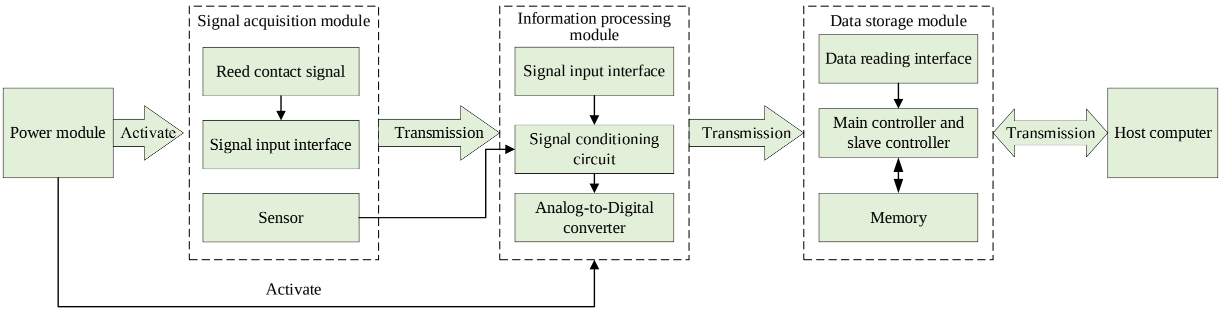

Figure 16. Schematic diagram of the storage testing system.

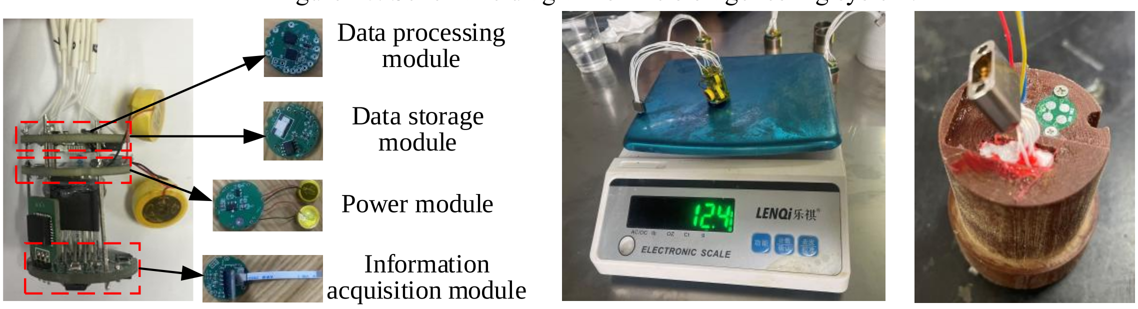

(a) Hardware composition of testing system (b) Test system weight (c) After potting

Figure 17. Physical hardware diagram of the testing system.

In Figure 17, (a) refers to the hardware and modules of the test system after installation, (b) refers to the physical quality of the hardware of the test system, and (c) refers to the test system after encapsulation. The system consists of three circular circuit boards, each 28 mm high and weighing 12.4 g. Considering the wiring size, the sealing height is 35 mm. After sealing, the wiring port is enclosed in the protective tube shell.

5.2. Experiment scheme

To ensure the drop angle of the projectile-like mechanical structure, vertical target shooting is used, with the gun positioned diagonally in front of the sandbag target, as shown in Figure 18.

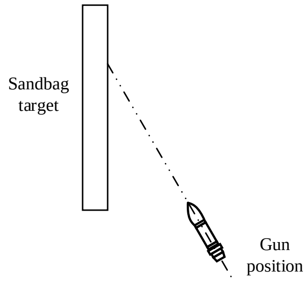

(a) Experimental layout

(b) Test Setup

Figure 18. Target position map of shooting range launching device positions.

In figure 18, (a) is a schematic diagram of the launching device and target positions; (b) is a figure of the launching device and target positions in the shooting range. Assemble the initiation actuation system on the grenade like mechanical structure for range testing, hitting the target with a sandbag of size 0.7 m × 0.3 m. The projectile-like mechanical structure has a drop angle of 30°, which can be adjusted by adjusting its position, and the impact speed is 330 m/s. After the shooting is complete, retrieve the projectile and obtain the start signal and the inertial block's movement arrival time.

The speed of the firing pin piercing the actuation component is measured using the contact indirect measurement method. The firing pin has a short travel inside the rotor. To ensure effective measurement of the firing pin piercing actuation component data, it is assumed that the firing pin moves uniformly inside the rotor. Install an elastic spring on the firing pin's stroke, connect the spring and firing pin to the circuit, and when the firing pin contacts the spring, the corresponding circuit will conduct. The principle and hardware installation diagram of this measurement method are shown in Figure 19.

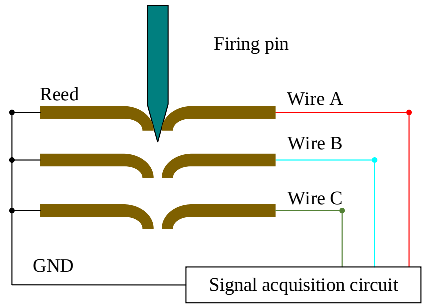

(a) Test Schematic

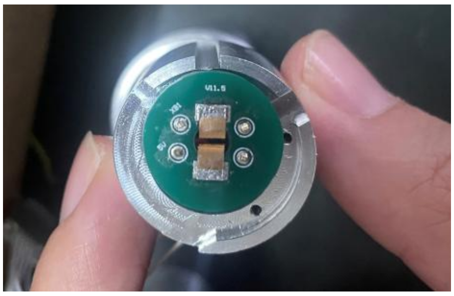

(b) Physical diagram

Figure 19. Firing pin speed measurement system.

Figure 19 (a) is the schematic diagram of the measurement method, and (b) is the corresponding hardware installation diagram. The reed is 0.2 mm thick, 10 mm long, and 4 mm wide. The startup of the inertial block can be determined from contact measurements. The principle is shown in Figure 20.

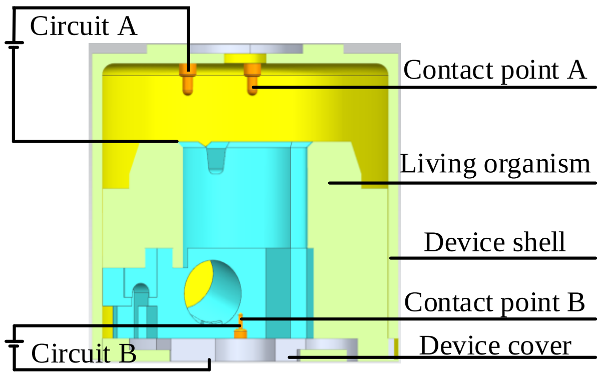

Figure 20. Schematic diagram of inertial block start-up measurement.

As shown in Figure 20, the conductivity status of circuit A and circuit B is detected through contact A and contact B, respectively, to determine the movement position of the inertial block and record the corresponding position time of the inertial block. Install the inertial block measurement system in the internal space of the actuation system. The installation of circuit A and circuit B is shown in Figure 21. Figure 21 (a) is the installation drawing of circuit A, (b) is the installation drawing of circuit B.

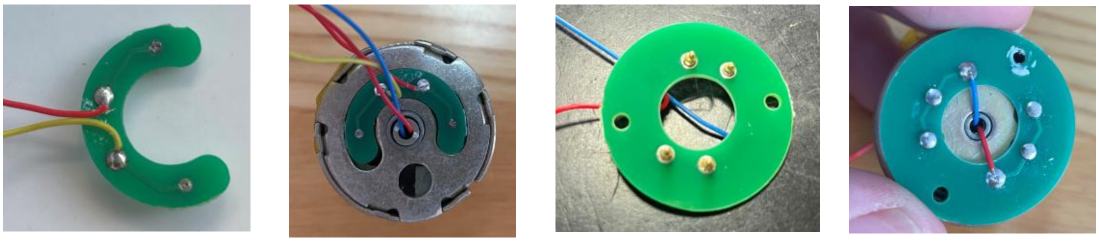

(a) Circuit A layout (b) Circuit A wiring (c) Circuit B layout (d) Circuit B wiring

Figure 21. Test system hardware.

Before the test range test, it is necessary to conduct a hammer impact test on the trigger device load testing system to verify its overload resistance and data acquisition accuracy. When a small, angled, projectile-like mechanical structure hits a sandbag with an overload of less than 5000 g, an impact overload of 6000 g is set to conduct an impact test on the firing pin speed testing system, as shown in Figure 22.

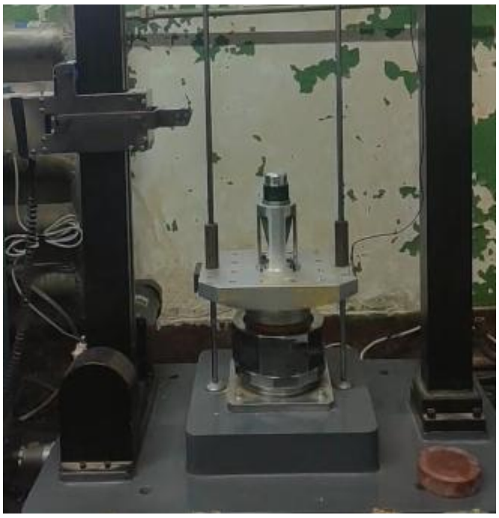

Figure 22. Impact test process.

5.3. Range testing

The measured firing pin velocity can be regarded as a direct manifestation of the transient shock vibration response of the actuation system under impact loading.

The test projectile-like mechanical structure is a howitzer sand projectile-like structure with a weight of 42.5 kg, and the velocity of the projectile-like mechanical structure hitting the target is 335 m/s. Two test projectiles were assembled with a test trigger device, and two were recovered. The test process is shown in Figure 23.

As shown in Figure 23, (a) shows the initial flight phase of the projectile-like structure leaving the launching device muzzle, (b) is the state of the projectile before hitting the target, (c) is the moment the projectile-like structure hits the sandbag, and (d) is the process of the projectile-like mechanical structure penetrating the sandbag.

The sandbag target before and after impact is shown in Figure 24.

(a) Initial flight phase (b) Before projectile-like mechanical hits the sandbag

(c) Projectile-like mechanical hits sandbag (d) Projectile-like mechanical penetrates sandbag

Figure 23. The test process was captured by high-speed cameras.

(a) Sandbag target before shooting (b) Sandbag target after shooting

Figure 24. Sandbag target before and after test.

From the process of the projectile-like mechanical structure, it can be seen that when the projectile-like mechanical structure hits the sandbag target, it will penetrate the sandbag target. Meanwhile, damage to sandbag targets is also limited to the radius of the incident point.

The comparison between the trigger device overload measured by the testing system and the simulated overload is shown in Figure 25.

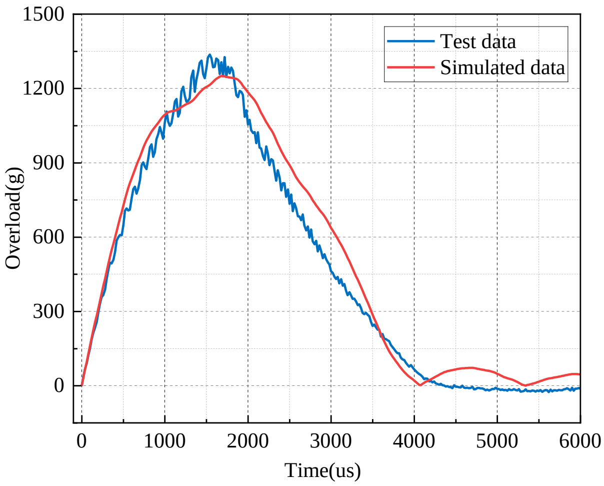

Figure 25. Test and simulation data of trigger device overload.

According to the overload curves of the trigger device from experiments and simulations, the simulated and experimental overloads are in good agreement in the rising phase and peak interval, and the simulations correctly predict the response amplitude and occurrence time. The main deviation occurs in the unloading tail stage, where simulation attenuation is faster, and the experimental tail is longer. The peak overload measured in the experiment is 1076 g, and the simulated peak overload is 1003 g, yielding a peak error of 6.78%. In the field of fuze and ammunition engineering, the generally recognized engineering allowable threshold of relative error for impact overload simulation is ⩽10%. The 6.78% peak error obtained in this study is well below this upper limit and fully meets the accuracy requirements for engineering design and reliability evaluation of the trigger device actuation system.

In-depth analysis of the discrepancy in tail attenuation between simulation and experiment is carried out, and the main causes are clarified as follows:

(1) Idealized setting of the target constitutive model in simulation: The sandbag target in the simulation is set with a non-reflective boundary around it and described by a uniform *MAT_SOIL_AND_FOAM constitutive model, which simplifies the multiple reflection and scattering of stress waves in the actual target. In the actual test, the plastic deformation and particle friction of the sandbag target after penetration will continue to consume energy, resulting in a longer vibration attenuation tail of the overload signal.

(2) Simplification of structural damping in the simulation model: The simulation model appropriately simplifies the secondary structural details of the projectile and trigger device, and ignores the additional damping caused by assembly clearance, contact surface friction, and microslip between parts in the actual assembly structure. These damping effects will slow the attenuation rate of the vibration signal during the unloading stage, resulting in a longer tail on the measured overload curve.

(3) Response characteristics of the actual test system: The storage test system used in the test has a certain low frequency response characteristic, which will lead to a slight tailing of the acquired overload signal in the unloading stage, while the simulation output signal is an ideal result without electrical noise and frequency response deviation, which is also an objective factor leading to the discrepancy in tail attenuation.

Among the two recovered test projectiles, the trigger device before optimizing the assembly variables m_2 and k_1 for projectile-like mechanical structure #2-1, and the trigger device before optimizing the assembly variables m_2 and k_1 for projectile-like mechanical structure # 2-2. The experimental results are shown in Table 4.

Table 4. Test results.

Bullet number	Variable symbol	Numerical value	Is the inertial block activated	Firing pin punching speed
2-1 (30°)	m_2 k_1	0.12 g 1.89 N/mm	Yes	27.53 m/s
2-2(30°)	m_2 k_1	0.118 g 1.97 N/mm	Yes	31.27 m/s

The measured firing pin velocity can be regarded as a direct manifestation of the transient shock–vibration response of the actuation system under impact loading. Capturing the activation of an inertial block indicates that the actuation system is functioning properly. When the speed of the firing pin piercing the actuation component is not less than 10.86 m/s, the actuation system can achieve activation. The test results show that the initial nominal variables are used for the # 2-1 projectile-like mechanical structure, with a measured piercing speed of 27.53 m/s, which is within the preoptimization simulation range of 24.96–32.93 m/s and meets the minimum activation speed requirement. The variables optimized by dynamic response analysis are used for projectile-like mechanical structure #2-2. where the actuation system completes reliable activation with a measured firing pin piercing speed of 31.27 m/s, which is within the post-optimization simulation range of 28.17–33.68 m/s. The optimized actuation system achieves a 13.6% improvement in piercing speed, consistent with the simulation-predicted optimization trend, verifying the effectiveness of the proposed dynamic response optimization scheme and further improving the reliability and stability of the actuation system.

In-depth analysis of the deviation between the measured values and the simulation nominal values is carried out, and the main sources of the deviation are clarified as follows:

(1) Idealized assumptions in the simulation model: The simulation adopts an ideal rigid-flexible contact model and ignores the random fluctuations of part surface roughness, assembly coaxiality error, and fit clearance in actual machining and assembly. These factors will lead to slight changes in friction resistance during the movement of the firing pin and inertial block, causing the actual speed to deviate from the simulation's nominal value.

(2) Heterogeneity of the target material: The sandbag target in the simulation is described by a uniform constitutive model, while the actual sandbag has spatial inhomogeneity in filling density and particle distribution, which leads to a slight difference between the actual impact overload input and the simulation input, and further affects the final piercing velocity.

(3) Systematic error of the measurement system: The contact-type velocity measurement method used in the test has a systematic measurement error of ±2%, which is an objective factor leading to the deviation between the measured value and the simulation value.

It should be emphasized that all measured velocities fall within the 95% confidence interval of the Monte Carlo simulation results, and the test optimization trend is completely consistent with the simulation, indicating that the above deviation does not affect the validity of the simulation model and the optimization conclusion.

6. Conclusion

This paper investigates the dynamic response characteristics of a projectile-like mechanical structure mechanical trigger device actuation system under impact loading, with particular emphasis on the firing pin piercing velocity, which is difficult to measure directly and is critical for determining whether the trigger device can reach the activation condition. Based on the mechanism analysis, a quantitative mathematical model of the key structural parameters and the puncture speed of the percussion needle was derived, and the influence of the percussion needle mass and spring stiffness on the system's dynamic response was explicitly characterized. LS-DYNA-ADAMS Monte Carlo cosimulation and range experiments are conducted to reveal the dynamic response law and the optimization effect of the actuation system. The main conclusions are as follows:

1. Under oblique impact, the firing pin dynamic response is dominated by radial friction and axial spring force, which are the core factors affecting the actuation reliability and provide a basis for reliability optimization.
2. The explicit quantitative mathematical model of the puncture speed and key structural parameters of the percussion needle was derived, and the influence of core parameters such as the quality of the percussion needle and the spring stiffness on the puncture speed was accurately characterized. The model's prediction results

were highly consistent with the simulation and test data, providing theoretical support for the parameter design and reliability evaluation of similar mechanical actuation systems. It was the core mechanical factor affecting the reliability of the actuation system and pointed out a clear direction for its reliability optimization.

3. By dynamically optimizing the firing pin mass and spring stiffness, by reducing the mass of the impact pin by 0.002 g and increasing the spring stiffness by 0.06 n/mm, and increasing the spring stiffness by 0.06 N/mm, the piercing velocity range is shifted to 28.17~33.68 m/s. The discrete fluctuation range of piercing velocity is reduced by 31%, the dynamic response consistency of the firing pin is significantly improved, and the anti-interference ability of the actuation system under complex impact working conditions is effectively enhanced.
4. Experimental results further demonstrate that the optimized firing pin parameters increase the piercing velocity from 27.53 m/s to 31.27 m/s, corresponding to an improvement of 13.6%. All measured velocities fall within the prediction interval of the Monte Carlo simulation, and the deviation between the measured values and the simulation nominal values is clarified through in-depth analysis of idealized simulation assumptions, target material heterogeneity, and measurement system error. This confirms the effectiveness and quantitative mathematical model of the proposed dynamic-response-oriented optimization strategy and validates the simulation method in capturing the transient impact and vibration behavior of the trigger device actuation system.
5. The proposed low-cost, high-precision joint simulation optimization framework is easy to implement in engineering. It can provide quantitative technical support for tolerance matching design and reliability forward optimization of fuze trigger core components, with strong practical engineering value.

References

1. Lin Z, Ning W. Study of fuze structure and reliability design based on the direct search method. IOP conference series. *Materials Science and Engineering* 2017; 187(1): 012038. https://doi.org/10.1088/1757-899x/187/1/012038.
2. Muhammad N, Fang Z, Shah S, Haider D. Reliability and remaining life assessment of an electronic fuze using accelerated life testing. *Micromachines* 2020; 11(3): 272. https://doi.org/10.3390/mi11030272.
3. Yang S, Wang Y, Luan D, Guo P. Research on numerical simulation of the instantaneity of a mechanical impact fuze. *Journal of Physics: Conference Series*; 2024; 2891(15): 152002. https://doi.org/10.1088/1742-6596/2891/15/152002.
4. Lou W Z, Feng H Z, Wang J K, Sun Y, Zhao Y C. Research on fuze microswitch based on corona discharge effect. *Defence Technology* 2021; 17(4): 1453-1460. https://doi.org/10.1016/j.dt.2020.08.002.
5. Kostka J. Malfunction investigation of the XM935 point detonating fuze. *Malfunction Investigation of the Xm935 Point Detonating Fuze* 1977. https://doi.org/10.21236/adb018406.
6. Corbin A. Fuze safety concepts. *Fuze Safety Concepts* 1970. https://doi.org/10.21236/ad0875185.
7. Zheng J, Li Y, Hu M, Wen J, Wang J, Kan J. Feasibility study of a miniaturized magnetorhological grease timing trigger as safety and arming device for spinning projectile. *Smart Materials and Structures* 2018; 27(11). https://doi.org/10.1088/1361-665x/aae5e7.
8. Heng A, Zhang S, Tan A, Mathew J. Rotating machinery prognostics: State of the art, challenges and opportunities. *Mechanical Systems and Signal Processing* 2009; 23(3): 724-739. https://doi.org/10.1016/j.ymssp.2008.06.009.
9. Teng D, Feng Y W, Chen J, Lu C. Structural dynamic reliability analysis: review and prospects. *International Journal of Structural Integrity* 2022; 13(5): 753-783. https://doi.org/10.1108/ijsi-04-2022-0050.
10. Zhao L, Yue P, Zhao Y, Sun S. Reliability analysis and optimization method of a mechanical system based on the response surface method and sensitivity analysis method. *Actuators* 2023; 12(12): 465. https://doi.org/10.3390/act12120465.
11. Liu R, Dobriban E, Hou Z, Qian K. Dynamic load identification for mechanical systems: A review. *Archives of Computational Methods in Engineering* 2021; (14): 1-33. https://doi.org/10.1007/s11831-021-09594-7.
12. Nie W, Xi Z, Xue W, Zhou Z. Study on inertial response performance of a micro electrical switch for fuze. *Defence Technology* 2013; 9(4): 187-192. https://doi.org/10.1016/j.dt.2013.11.001.

13. Qin Y, Li Y, Liu Y, Che D, Zou X, Ma X. Design and test of MEMS setback arming device for fuze. *IEEE Access* 2026; 14: 8687-8698. https://doi.org/10.1109/ACCESS.2026.3653758.
14. Yu D, Yang B, Yan K, Li C, Ma X, Han X, Zhang H, Dai K.. Dynamic transfer model and applications of a penetrating projectile–fuze multibody system. *International Journal of Mechanical System Dynamics* 2023; 3(4): 360-372. https://doi.org/10.1002/msd2.12092.
15. Zhang S, Rui X, Yu H, Dong X. Study on the coupling calculation method for the launch dynamics of a self-propelled artillery multibody system considering engraving process. *Defence Technology* 2024, 39: 67-85. https://doi.org/10.1016/j.dt.2024.04.011.
16. Chang T, Wen Q, Wang Y, Wang G, Jiang C, Yan L. Finite element evaluation of key approaches to develop insensitive fuze. *Journal of Thermal Science and Engineering Applications* 2021; 13(4): 041004. https://doi.org/10.1115/1.4048759.
17. Lei S, Cao Y, Nie W, Xi Z, Yao J, Zhu H, Lu H. Research on mechanical responses of a novel inertially driven MEMS safety and arming device under dual-environment inertial loads. *IEEE Sensors Journal* 2022; 22(8): 7645-7655. https://doi.org/10.1109/jsen.2022.3157054.
18. Chen L, Hao Y, Wang X, Xin S, Feng M. Design of small caliber fuze electrothermal MEMS security mechanism. In: *Proceedings of the International Conference on Information Control, Electrical Engineering and Rail Transit: ICEERT 2023*, Volume 1; 2025: Springer Nature. https://doi.org/10.1007/978-981-97-4620-0_31.
19. He B, Yuan Y, Ren J, Lou W, Feng H, Zhang M, Lv S, Su W. A high-functional-density integrated inertial switch for super-quick initiation and reliable self-destruction of a small-caliber projectile fuze. *Micromachines* 2023; 14(7): 1377. https://doi.org/10.3390/mi14071377.
20. Sharp A, Andrade J, Ruffini N. Design for reliability for the high reliability fuze. *Reliability Engineering & System Safety* 2019; 181: 54-61. https://doi.org/10.1016/j.ress.2018.04.032.
21. Liu J, Qi X, Jia J, Fu B. Study on the reliability problem of MEMS fuze mechanism. *Advanced Materials Research* 2013; 628: 72-77. https://doi.org/10.4028/www.scientific.net/AMR.628.72.
22. Xiao X, Feng S, Gao Y, Zhang B. Trajectory prediction of rigid projectile for oblique penetration into multi-layer aluminum targets. *International Journal of Impact Engineering* 2024; 190: 104967. https://doi.org/10.1016/j.ijimpeng.2024.104967.
23. Liang C, Shen Q, Deng Z, Li H, Liang D. An improved particle filtering projectile trajectory estimation algorithm fusing velocity information. *Measurement* 2025; 241(000): 115749. https://doi.org/ 10.1016/j.measurement.2024.115749.
24. Hui J, Gao M, Li M, Li M, Zou H, Zhou G. Multi-objectives nonlinear structure optimization for actuator in trajectory correction fuze subject to high impact loadings. *Defence Technology* 2021; 17(4): 1338-1351. https://doi.org/10.1016/j.dt.2020.07.004.
25. Fang S, Zhang S, Xu Z. Study on structure design of an safety detonating fuze for underwater depth bomb. *Journal of Projectiles, Rockets, Missiles and Guidance* 2023; 43(3): 99-105. https://doi.org/10.15892/j.cnki.djzdxb.2023.03.015.
26. Qin Y, Shen Y, Zou X, Hao Y. Simulation and test of a MEMS arming device for a fuze. *Micromachines* 2022; 13(8): 1161. https://doi.org/10.3390/mi13081161.
27. Qin Y, Shen Y, Zou X, Hao Y. Test and improvement of a fuze MEMS setback arming device based on the EDM Process. *Micromachines* 2022; 13(2): 292. https://doi.org/10.3390/mi13020292.
28. Xu P, Zhao N, Shi K, Cui S, Chen C, Liu J. Theoretical and numerical study on dynamic response of propellant actuator. *Actuators* 2022; 11(11): 314. https://doi.org/10.3390/act11110314.
29. Yang B, Dai K, Li C, Yu D, Zhang A, Cheng J Z, Zhang H. Lightweight recoverable mechanical metamaterials for efficient buffering of continuous multi extreme impacts. *Sustain. Materials Technologies* 2024; 39: e00839. https://doi.org/10.1016/j.susmat.2024.e00839.
30. He Y, Zhang A, Liu F, Han X, Zhou D. Reliability loss–oriented product assembling quality risk modeling approach based on reliability–quality–reliability chain. *Proceedings of the Institution of Mechanical Engineers, Part B Journal of Engineering Manufacture.* 2020 234(10): 095440542091129. https://doi.org/10.1177/0954405420911294.
31. Xu P, Cui S, Zhao N, Zhang B. Theoretical analysis of mechanical and damage behavior of fuze structure under near-field blast load. *Nonlinear Dynamics* 2025; 113: 16367-16381. https://doi.org/10.1007/s11071-025-11017-2.
32. Xie R, Ren X, Liu L, Xue Y, Fu D, Zhang R. Research on design and firing performance of Si-based detonator. *Defence Technology* 2014; 10(1): 34-39. https://doi.org/10.1016/j.dt.2014.01.002.
33. Shi X, Pan J, Li J, Jiang C, Zhu Y, Quaye E. Effect of obstacles behind the pre-detonator tube on the re-initiation of diffracted detonation wave. *International Journal of Hydrogen Energy* 2023; 48(12): 4860-4874. https://doi.org/10.1016/j.ijhydene.2022.11.012.
34. Jiang Q, Zhang Y, Liu Y, Xu R, Zhu J, Wang J. Structural optimization of serpentine channel water-cooled plate for lithium-ion battery

modules based on multi-objective bayesian optimization algorithm. *Journal of Energy Storage* 2024; 91: 112136. https://doi.org/10.1016/j.est.2024.112136.

35. Chen S, Zhang S. A structural optimization algorithm with stochastic forces and stresses. *Nature Computational Science* 2022; 2(11): 736-744. https://doi.org/10.1038/s43588-022-00350-w.
36. Prokhorenko S, Kalke K, Nahas Y, Bellaiche L. Large scale hybrid Monte Carlo simulations for structure and property prediction. *npj Computational Materials* 2018; 4(1): 80. https://doi.org/10.1038/s41524-018-0137-0.
37. Ceperley D, Jensen S, Yang Y, Niu H, Pierleoni C, Holzmann M. Training models using forces computed by stochastic electronic structure methods. *Electronic Structure* 2024; 6(1): 015011. https://doi.org/10.1088/2516-1075/ad2eb0.
38. Ma S, He G, Yan K, Li W, Zhu Y, Hong J. Structural optimization of ball bearings with three-point contact at high-speed. *International Journal of Mechanical Sciences* 2022; 229: 107494. https://doi.org/10.1016/j.ijmecsci.2022.107494.
39. Chen Y, Chen H, Zeng H, Zhu J, Chen K, Cui Z, Wang J. Structural optimization design of sinusoidal wavy plate fin heat sink with crosscut by Bayesian optimization. *Applied Thermal Engineering* 2022; 213: 118755. https://doi.org/10.1016/j.applthermaleng.2022.118755.
40. Zhang C, Tao M, Wang C, Yang C, Fan J. Differentiable automatic structural optimization using graph deep learning. *Advanced Engineering Informatics* 2024; 60: 102363. https://doi.org/10.1016/j.aei.2024.102363.
41. Li, K, Ye W. Improving efficiency in structural optimization using RBFNN and MMA-Adam hybrid method. *Advanced Engineering Informatics* 2024; 62: 102869. https://doi.org/10.1016/j.aei.2024.102869.
42. Payette M, Abdul-Nour G. Machine learning applications for reliability engineering: A review. *Sustainability* 2023; 15(7): 6270. https://doi.org/10.3390/su15076270.
43. Lee J, Singh J, Azamfar M, Pandhare V. *Industrial AI and predictive analytics for smart manufacturing systems.* In: Smart Manufacturing. Amsterdam: Elsevier; 2020. p. 213-244.